

MIT Open Access Articles

A procedure for testing the significance of orbital tuning of the martian polar layered deposits

The MIT Faculty has made this article openly available. **Please share** how this access benefits you. Your story matters.

Citation: Sori, Michael M. et al. "A Procedure for Testing the Significance of Orbital Tuning of the Martian Polar Layered Deposits." *Icarus* 235 (2014): 136–146.

As Published: <http://dx.doi.org/10.1016/j.icarus.2014.03.009>

Publisher: Elsevier

Persistent URL: <http://hdl.handle.net/1721.1/110320>

Version: Author's final manuscript: final author's manuscript post peer review, without publisher's formatting or copy editing

Terms of use: Creative Commons Attribution-NonCommercial-NoDerivs License



1 A procedure for testing the significance of orbital tuning of the
2 Martian polar layered deposits

3
4 Michael Sori¹, J. Taylor Perron¹, Peter Huybers², Oded Aharonson³

5
6 ¹ Department of Earth, Atmospheric and Planetary Sciences, Massachusetts Institute of
7 Technology, Cambridge, Massachusetts, USA

8 ² Department of Earth and Planetary Sciences, Harvard University, Cambridge,
9 Massachusetts, USA

10 ³ Department of Geological and Planetary Sciences, California Institute of Technology,
11 Pasadena, California, USA

12
13
14

15 **ABSTRACT:**

16 Layered deposits of dusty ice in the Martian polar caps have been hypothesized to
17 record climate changes driven by orbitally induced variations in the distribution of
18 incoming solar radiation. Attempts to identify such an orbital signal by tuning a
19 stratigraphic sequence of polar layered deposits (PLDs) to match an assumed forcing
20 introduce a risk of identifying spurious matches between unrelated records. We present
21 an approach for evaluating the significance of matches obtained by orbital tuning, and
22 investigate the utility of this approach for identifying orbital signals in the Mars PLDs.
23 Using a set of simple models for ice and dust accumulation driven by insolation, we
24 generate synthetic PLD stratigraphic sequences with nonlinear time-depth relationships.
25 We then use a dynamic time warping algorithm to attempt to identify an orbital signal in
26 the modeled sequences, and apply a Monte Carlo procedure to determine whether this
27 match is significantly better than a match to a random sequence that contains no orbital

28 signal. For simple deposition mechanisms in which dust deposition rate is constant and
29 ice deposition rate varies linearly with insolation, we find that an orbital signal can be
30 confidently identified if at least 10% of the accumulation time interval is preserved as
31 strata. Addition of noise to our models raises this minimum preservation requirement, and
32 we expect that more complex deposition functions would have a similar effect. In light of
33 these results, we consider the prospects for identifying an orbital signal in the actual PLD
34 stratigraphy, and conclude that this is feasible even with a strongly nonlinear relationship
35 between stratigraphic depth and time, provided that a sufficient fraction of time is
36 preserved in the record and that ice and dust deposition rates vary predictably with
37 insolation.

38

39 **1. Introduction**

40 The topographic domes of the north and south polar ice caps on Mars are mostly
41 composed of kilometers-thick layered sedimentary deposits, the polar layered deposits
42 (PLDs), which are exposed in spiraling troughs cut into the caps [Murray et al., 1972;
43 Cutts, 1973; Howard et al., 1982; Byrne, 2009], as shown in Figure 1. The PLDs were
44 initially seen in images from the Mariner 9 spacecraft [Murray et al., 1972], and were
45 immediately inferred to be composed of atmospherically deposited dust and ice [Cutts,
46 1973]. Since then, the PLDs have been more thoroughly characterized. Carbon dioxide
47 ice and clathrate hydrate have been shown to be compositionally insignificant based on
48 their effects on thermal properties [Mellon, 1996] and bulk strength [Nye et al., 2000].
49 Water ice dominates dust volumetrically; dust volume composition has an upper limit of
50 2% in the north polar cap [Picardi et al., 2005] and 10% in the south polar cap [Plaut et

51 al., 2007] according to MARSIS radar transparency data, and ~15% in the south polar
52 cap according to gravity anomalies associated with the area [Zuber et al., 2007;
53 Wieczorek et al., 2008]. Concentrations far smaller than these upper bounds could
54 produce the observed brightness differences [Cutts, 1973]. MOLA topography
55 demonstrates that the ice caps are dome-like structures 3-4 km thick [Zuber et al., 1998],
56 with volumes of 1.14 million km³ for the northern dome [Smith et al., 2001] and 1.6
57 million km³ for the southern dome [Plaut et al., 2007]. The deposits are locally overlain
58 by seasonal carbon dioxide frost [Smith et al., 2001]. Radar soundings from the
59 SHARAD instrument [Phillips et al., 2008] have revealed that large-scale stratigraphy is
60 similar in different parts of the northern ice cap, implying that the PLDs record regional
61 or global climate phenomena rather than local conditions.

62 Many authors have attempted to constrain the deposition rates of polar ice or dust
63 [Pollack et al., 1979; Kieffer, 1990; Herkenhoff and Plaut, 2000], but these estimates
64 span orders of magnitude. Populations of impact craters on the polar caps provide some
65 constraints, including an estimated mean surface age of 30 to 100 Myr for the southern
66 PLDs [Koutnik et al., 2002] and an estimated upper limit on the accumulation rate of 3-4
67 mm/yr for the northern PLDs [Banks et al., 2010]. Despite these efforts, the ages of the
68 PLDs remain poorly constrained.

69 It has been proposed that patterns in the thickness and brightness of these layers,
70 which are thought to result from variable dust concentration in the ice, are controlled by
71 changes in the distribution of solar radiation due to quasi-periodic variations in the
72 planet's spin and orbital characteristics over time, specifically climatic precession,
73 obliquity variation, and eccentricity variation [Murray et al., 1973; Cutts et al., 1976;

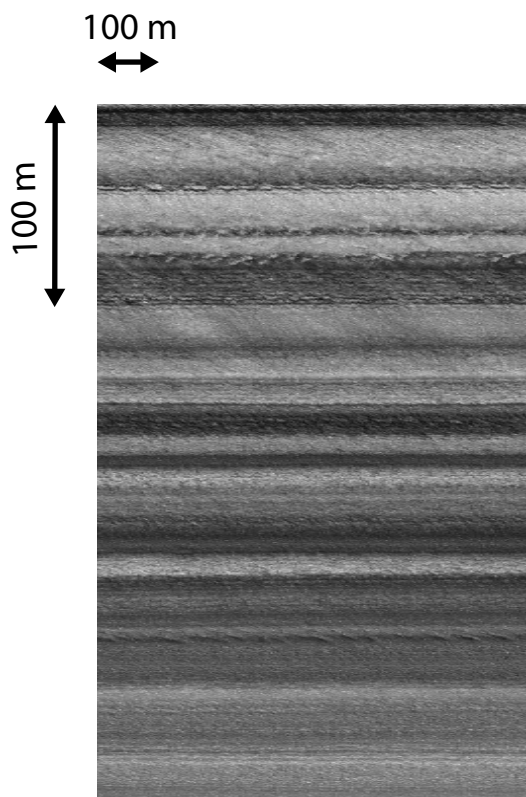


Figure 1. Mars Orbiter Camera (MOC) Image #M0001754 of a PLD stratigraphic sequence, corrected for topography. The vertical scale corresponds to vertical depth within the PLD sequence, and the horizontal scale corresponds to distance along the outcrop.

74 Toon et al., 1980; Cutts and Lewis, 1982; Howard et al., 1982; Thomas et al., 1992,
75 Laskar et al., 2002; Milkovich and Head, 2005; Milkovich et al., 2008; Fishbaugh et al.,
76 2010]. In this way, the PLDs may record past Martian climate.

77 An analogous argument is often made regarding ice cores or marine sediment
78 cores and Earth's paleoclimate. Some of the variability in marine Pleistocene
79 paleoclimate proxies has been convincingly linked to orbital changes [Hays et al., 1976].
80 However, there is debate about how much of the recorded climate variability was
81 deterministically controlled by Milankovitch cycles [Kominz and Pisias, 1979; Wunsch,
82 2004]. In theory, the problem on Mars should be more tractable than the analogous
83 problem on Earth. The Martian atmosphere is orders of magnitude less massive than

84 Earth's, and Mars has not had a surface ocean in the recent past, two factors that should
85 make the Martian climate system simpler than the terrestrial one. Mars also experiences
86 larger obliquity and eccentricity variations than Earth [Ward, 1973; Touma and Wisdom,
87 1993; Laskar et al., 2004], which should make an orbital signal, if present, stronger and
88 perhaps easier to detect.

89 Despite the likelihood of a simpler climate on Mars, detection of an orbital signal
90 in the PLDs is not a trivial task. The relationship between time and stratigraphic depth in
91 the PLDs is unknown, and is likely nonlinear. There are no absolute ages available for
92 any part of the deposits. Image brightness may contain noise from image artifacts,
93 inherent noise in the deposition rates of ice and/or dust, and an indirect relationship
94 between visible albedo and PLD composition [Tanaka, 2005; Fishbaugh and Hvidberg,
95 2006; Herkenhoff et al., 2007; Levrard et al., 2007]. Because of these complexities and
96 uncertainties, detection of an orbital signal in the Martian PLDs using spacecraft
97 observations poses a considerable challenge [Perron and Huybers, 2009].

98 The problem of orbital signal detection has been considered almost since the
99 PLDs were first discovered. Given the lack of an absolute chronology, most efforts to
100 interpret the PLDs have focused on modeling or analyzing their stratigraphy. The first
101 study to consider in detail how different PLD formation mechanisms influence the
102 resulting stratigraphy was that of Cutts and Lewis [1982]. They considered two
103 deposition models. In their first model, material composing the major constituent of the
104 PLDs is deposited at a constant rate, and differences between layers are caused by a
105 minor constituent that is deposited at a constant rate only when the obliquity of the planet
106 is below a certain threshold value. In their other model, only one type of material is

107 deposited, but only when the obliquity is below a certain threshold value; layer
108 boundaries correspond to periods with no deposition. Although these models are highly
109 simplified, their work revealed the sensitivity of PLD stratigraphy to factors such as ice
110 deposition rates and thresholds, and thus hinted at the difficulty of detecting an orbital
111 signal. More recently, Levrard et al. [2007] used a global climate model for Mars to study
112 ice accumulation rates and concluded that formation of PLD layers must indeed be more
113 complex than originally modeled.

114 Other authors have used time series analysis to search for coherent signals in the
115 PLD stratigraphy, particularly signals that may be related to orbital forcing. Milkovich
116 and Head [2005] analyzed spectra of brightness profiles through the north PLDs, and
117 reported the presence of a signal with a 30 m vertical wavelength in the upper 300 m of
118 the PLDs, which they interpreted as a signature of the approximately 51 kyr cycle of the
119 climatic precession. They assumed a linear time-depth relationship, however, and did not
120 evaluate the statistical significance of the signal they identified. Perron and Huybers
121 [2009] expanded this analysis, also assuming a linear time-depth relationship on average,
122 but allowing for local variability (“jitter”) in this relationship. They also evaluated the
123 significance of peaks in the PLD spectra with respect to a noise background. Perron and
124 Huybers [2009] found that the PLD spectra closely resemble spectra for autocorrelated
125 random noise, but that many stratigraphic sequences contain intermittent, quasi-periodic
126 bedding with a vertical wavelength of 1.6 m. Subsequent studies have confirmed and
127 refined this measurement of 1.6 meter bedding through analyses of higher-resolution
128 imagery and stereo topography [Fishbaugh, 2010; Limaye et al., 2012].

129 These applications of conventional time series analysis techniques have revealed
130 signals within the stratigraphy, but have not been able to conclusively identify evidence
131 of orbital forcing due to the absence of multiple periodic signals with a ratio of
132 wavelengths that matches the expected ratio of orbital periods [Perron and Huybers,
133 2009]. They have also been limited by the assumption of a linear time-depth relationship,
134 a scenario that, while possible, is rare in terrestrial stratigraphic sequences [Sadler, 1981;
135 Weedon, 2005]. Thus, while the Mars polar caps do appear to record repeating regional
136 or global climate events, the duration of these events and their relationship to orbitally
137 forced variations in insolation remain unknown.

138 In studies of terrestrial paleoclimate records, it is common to address the problem
139 of unknown time-depth relationships by tuning an observed record – adjusting its time
140 model nonuniformly by moving points in the record closer together or further apart – to
141 match an assumed forcing with a known chronology, or by tuning two or more observed
142 records with unknown chronologies to match each other. There have been limited efforts
143 to apply tuning procedures to the Mars PLDs. Laskar et al. [2002] compared the PLD
144 stratigraphy with an insolation time series using an approach in which a portion of the
145 photometric brightness image was stretched to provide an approximate fit to the
146 insolation time series. They analyzed only one image, however, and did not evaluate the
147 goodness of fit statistically. Milkovich et al. [2008] used the signal-matching algorithm of
148 Lisiecki and Lisiecki [2002] to search for stratigraphic correlations between PLDs in
149 different regions of the north polar cap, but did not attempt to tune PLD sequences to
150 match insolation records.

151 The need to assess the statistical significance of proposed tunings is widespread in
152 the study of terrestrial paleoclimate [Proistosescu et al., 2012] and in other analyses that
153 seek correlations among time series with uncertain chronologies. The essential problem is
154 that any effort to tune records to match one another will produce some agreement, but it
155 is not clear whether this agreement arose by chance, or whether it reveals an underlying
156 relationship. To address this need, methods have been proposed that estimate the
157 significance of a tuned fit between records, generally by comparing the fit between
158 records that are hypothesized to share an underlying relationship with fits to random
159 records that share no underlying relationship with the observed record. This was the
160 general approach adopted by Milkovich et al. [2008] in their effort to correlate PLD
161 stratigraphic sequences with one another.

162 In this paper, we adapt a statistical procedure for evaluating the significance of
163 orbital tuning that has been successfully applied to terrestrial paleoclimate records and
164 has been shown to be applicable to comparisons between any two time-uncertain series
165 [Haam and Huybers, 2010]. We use the procedure to compare two data series –
166 insolation as a function of time and composition of strata as a function of depth – and
167 assess the potential for detecting an orbital signal in the Mars polar layered deposits. Our
168 approach is divided into two main steps. First, we construct simplified models for PLD
169 accumulation and drive these models with a Martian insolation time series to create
170 synthetic PLD records. We consider three different models, none of which produces a
171 linear time-depth relationship. In the second step, we perform a statistical analysis to
172 determine how reliably we can detect the orbital signal in the synthetic PLD records. The
173 statistical analysis uses a dynamic time warping algorithm to tune the synthetic PLD

174 records to the insolation time series and a Monte Carlo procedure that evaluates the
175 statistical significance of that tuning by applying the same dynamic time warping
176 algorithm to random signals. For each modeled PLD formation mechanism, this
177 procedure yields an estimated confidence level for detection of an orbital signal. We then
178 consider the implications of this analysis for the interpretation of the PLD stratigraphic
179 sequences measured from spacecraft observations, including the prospects for identifying
180 evidence of orbital forcing. The purpose of our work is not to definitively identify the
181 accumulation function controlling PLD formation, but to assess the performance of a
182 technique that can be used to analyze PLD records that do not have a linear depth-age
183 relationship.

184

185 **2. Polar Layered Deposit Formation Models**

186 *2.1 Insolation forcing*

187 In the models presented here, hypothetical ice and dust deposition rates expressed
188 as functions of insolation are integrated forward in time to produce synthetic PLD
189 stratigraphic sequences. Changes in the seasonality and global distribution of insolation
190 on Mars are controlled mainly by the planet's climatic precession, obliquity variations,
191 and eccentricity variations [Ward, 1973, 1974, 1992; Touma and Wisdom, 1993; Laskar
192 et al., 2004]. The climatic precession of Mars has a period of approximately 51 kyr. The
193 obliquity of Mars varies with an average period of 120 kyr due to variation of the spin
194 axis and is modulated by a 1200 kyr period due to variation of its orbital inclination
195 [Ward, 1973]. The eccentricity of Mars's orbit varies with periods of 95 kyr, 99 kyr and
196 2400 kyr [Laskar et al., 2004].

197 The evolution of Martian orbital parameters over long time intervals is chaotic
198 [Laskar and Robutel, 1993; Touma and Wisdom, 1993]. Given the precision with which
199 present-day orbital parameters can be measured, the current solution for insolation over
200 time [Laskar et al., 2004] is accurate for the last 10-20 Myr. We calculate insolation over
201 this interval from the orbital solution of Laskar et al. [2004] using methods described by
202 Berger [1978]. Like previous analyses of the PLDs [Laskar et al., 2002], we use the
203 average daily insolation at the north pole on the summer solstice (Fig. 2) as a proxy for
204 the climatic conditions controlling the deposition of polar ice and dust. This assumes that
205 the effect of the axial precession on the magnitude of ice deposition in a given year is less
206 important than the effect of obliquity. As noted above, our objective in this study is to
207 evaluate a procedure for analyzing PLD sequences with nonlinear time-depth
208 relationships, not to identify the exact relationship between insolation and PLD
209 formation, so our results do not rely on the correctness of this assumption.

210 The orbital solution features a significant reduction in mean obliquity, and
211 therefore summer insolation at the poles, after approximately 5 Ma. Paleoclimate models
212 suggest that polar ice caps would not have been stable before this time [Jakosky et al.,
213 1995; Mischna et al., 2003; Forget et al., 2006; Levrard et al., 2007], which would imply
214 that the PLDs exposed in the upper portions of the ice caps are younger than 5 Ma.
215 However, other studies have estimated the age of the southern PLDs to be an order of
216 magnitude older than this, which may be related to protective lag deposits [Banks et al.,
217 2010]. There is an observational constraint from crater counts that yields a maximum age
218 of ~1 Ga on the north polar basal units [Tanaka et al., 2008], and our approach does not

219 depend on an estimate of the absolute age of the PLDs. In the models presented here, we
 220 only consider the past five million years of Martian insolation history (Fig. 2).

221

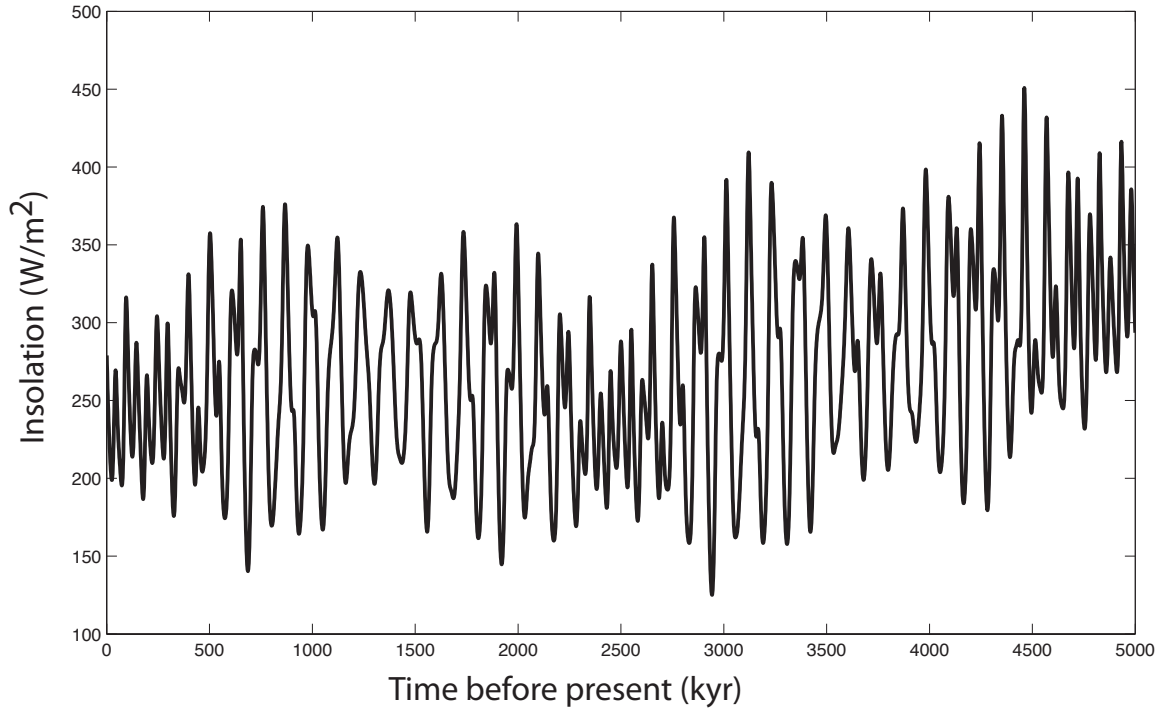


Figure 2. Martian insolation over the past five million years at the north pole on the summer solstice, calculated from the orbital solution of Laskar et al. [2004].

222

223

224 *2.2 Ice and dust accumulation*

225 We consider three classes of PLD formation models, which are illustrated
 226 schematically in Figure 3. Although our models are more complicated than those
 227 originally studied by Cutts and Lewis [1982], they are not intended to capture all aspects
 228 of the physical processes controlling ice and dust deposition rates. The key attribute of
 229 our simple, insolation-driven models is that they produce strata with a non-linear time-
 230 depth relationship, and therefore provide a useful tool for exploring how insolation

231 forcing may be recorded in the PLDs. In each model, dust deposition rate f_{dust} [L/T] is
 232 held constant, and ice deposition rate f_{ice} [L/T] is expressed as a simple function of
 233 insolation, ϕ (W/m^2). In the first model, ice deposition rate $f_{\text{ice}}(\phi)$ varies

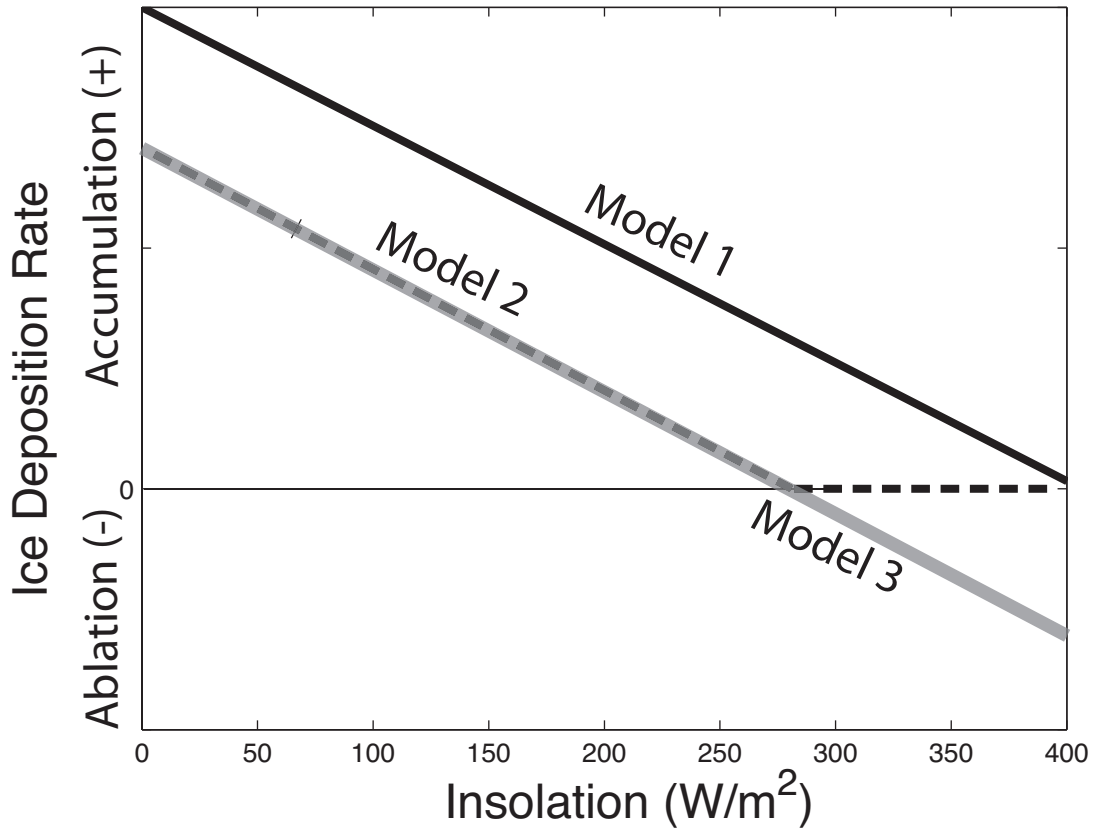


Figure 3. Ice deposition rate (arbitrary units) as a function of insolation for the three models considered. Model 1 (solid black line) is a simple linear dependence of deposition rate on insolation, with no hiatuses in deposition. Model 2 (dotted line) allows ice deposition rate to drop to zero at high insolation values, creating hiatuses. Model 3 (solid gray line) allows ice deposition rate to become negative at high insolation values, causing ablation of existing layers.

234

235 linearly with insolation. Higher insolation corresponds to slower ice deposition. The
 236 insolation value at which no ice is deposited ($f_{\text{ice}}(\phi) = 0$) is chosen to be greater than the
 237 maximum insolation reached in the past five million years, so that $f_{\text{ice}}(\phi)$ is always
 238 positive, and the resulting PLDs contain no hiatuses in accumulation.

239 The second model is the same as the first model, except that the insolation at
240 which $f_{\text{ice}}(\phi) = 0$ is chosen to be less than the maximum insolation reached in the past five
241 million years. For insolation values above this threshold, $f_{\text{ice}}(\phi) = 0$. Therefore, for
242 certain time intervals in the past five million years, no ice is deposited, and the resulting
243 PLDs contain hiatuses in accumulation.

244 The third model is the same as the second model, except that $f_{\text{ice}}(\phi)$ maintains its
245 linear relationship with insolation at all insolation values, which means that $f_{\text{ice}}(\phi)$ is
246 negative for insolation values above the threshold. A negative ice deposition rate
247 corresponds to ablation, which destroys a previously deposited section of the PLD. The
248 resulting PLDs therefore contain hiatuses, as in the second model, but the hiatuses are not
249 limited to time intervals when insolation exceeds a threshold value. Figure 3 summarizes
250 the ice deposition functions for the three models. All three models can have their
251 parameters adjusted in order to vary the absolute values of their deposition rates. The
252 units of brightness and depth in the models are arbitrary, so the slopes of the trends
253 relating deposition rate to insolation in Figure 3 do not affect our tuning procedure.

254

255 *2.3 Generation of synthetic stratigraphic sequences*

256 For each instance of a model, the insolation time series (Fig. 2) is sampled every
257 1000 years, for a total of 5000 time steps. At every time step, ice and dust deposition
258 rates are calculated, an increment of ice is deposited using a forward Euler method, and
259 the dust concentration of the ice is calculated as the ratio of the dust and ice deposition
260 rates. This iterative procedure constructs a synthetic PLD stratigraphic sequence

261 consisting of a series of “beds” of unequal thickness and variable dust concentration.

262 Figure 4 shows examples of outputs for each model class.

263 The models make a number of simplifications. Dust is assumed to be
264 volumetrically negligible, on the basis of work that suggests an upper limit for dust
265 content of 2% by volume for the northern polar cap [Picardi et al., 2005]. Dust is
266 assumed to blow away during hiatuses in ice deposition, such that dust lags do not
267 develop in models with hiatuses or ablation. This assumption is consistent with abundant
268 evidence for eolian sediment transport in the north polar region [Byrne, 2009]. We
269 neglect topographic differences involving aspect and shadowing that could potentially
270 cause local variations in deposition rates, based on the observation that large-scale
271

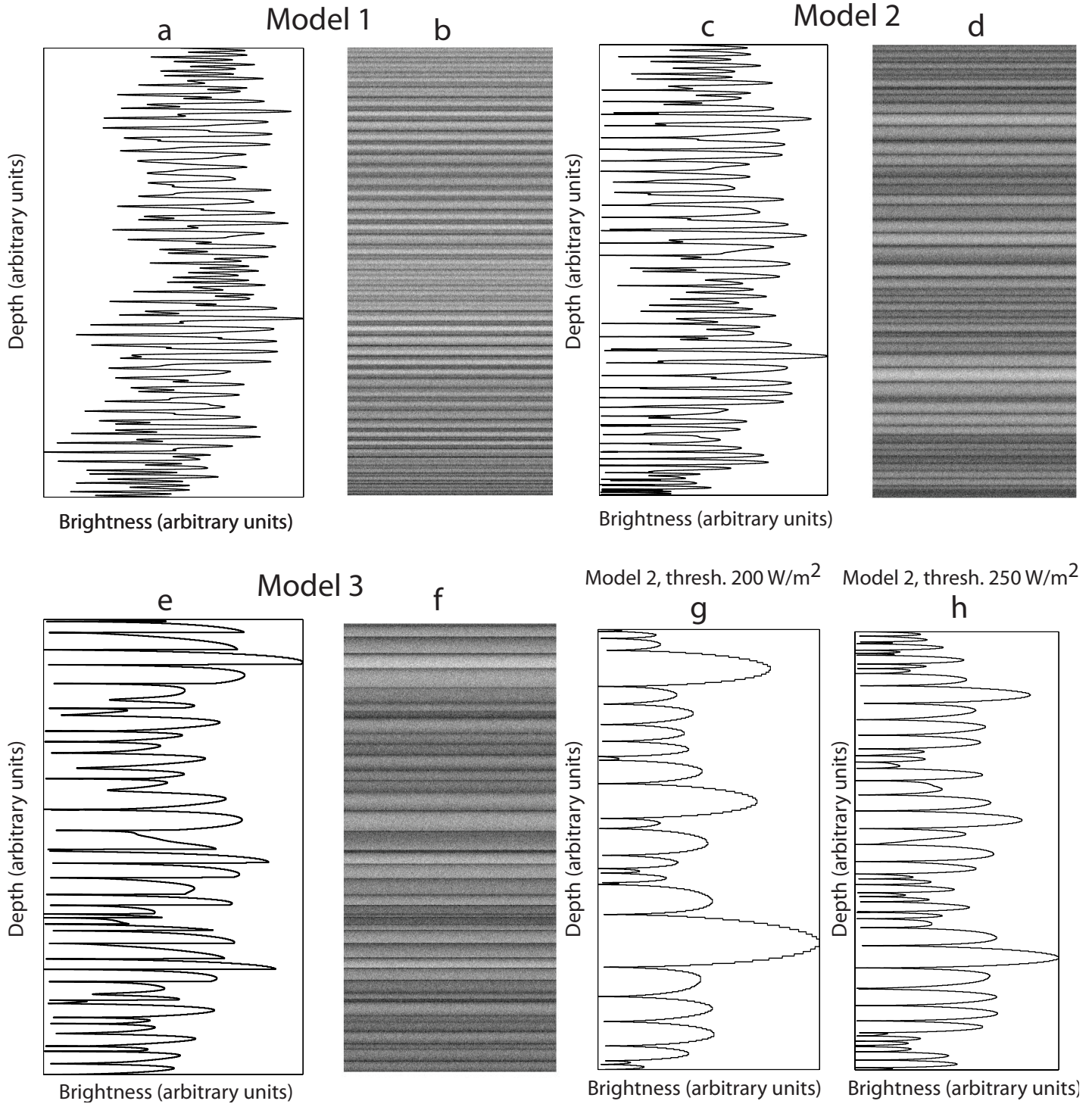


Figure 4. Examples of synthetic PLD stratigraphic sequences produced by the three model classes. Plots in (a,c,e) show dust concentration in arbitrary units as a function of depth in arbitrary units. Images in (b,d,f) show simulated images of the stratigraphy (compare with Fig. 1) created by assuming that brightness scales inversely with dust concentration and adding Gaussian noise. The third model class (e,f), which includes ablation, produces synthetic PLDs most visually similar to actual images. Plots in (g,h) were both produced by the model with hiatuses and no ablation, but with different values of the threshold insolation for ice accumulation: 200 W/m^2 in (g), 250 W/m^2 in (h).

272

273 stratigraphy is consistent across the polar ice caps [Phillips et al., 2008]. In this study, we
274 have chosen to ignore insolation-induced variations in dust deposition rate, because we
275 expect ice deposition to be more strongly influenced by insolation [Toon et al., 1980].
276 Dust deposition rate is likely to be affected by global dust storms, which may correlate
277 with insolation [Zurek and Martin, 1993], but in the absence of a clear expectation for the
278 relationship between insolation and dust, and given the evidence that atmospheric
279 dustiness varies considerably over intervals much shorter than the periods of orbital
280 changes [Zurek and Martin, 1993], the relation between insolation and ice deposition rate
281 is a logical starting point. Stratigraphic thickness and dust concentrations are presented
282 in arbitrary units, because long-term deposition rates of ice and dust are poorly
283 constrained, with estimates spanning three orders of magnitude [Pollack et al., 1979;
284 Kieffer, 1990; Herkenhoff and Plaut, 2000]. This does not pose a problem for the tuning
285 procedure described below, because potential detection of an orbital signal involves
286 consideration of the relative amplitudes and frequencies of stratigraphic signals in PLD
287 records rather than the absolute dust concentrations and stratigraphic distances.

288

289 **3. Statistical Analysis**

290 Our statistical analysis consists of two main components: a dynamic time warping
291 algorithm that tunes a synthetic PLD record in an effort to match the insolation function,
292 and a Monte Carlo procedure that evaluates the statistical significance of the match.

293

294

295

296 *3.1 Orbital tuning by dynamic time warping*

297 Dynamic time warping (DTW) allows for the possibility that the PLDs do not
298 follow a linear time-depth relationship. We use a DTW algorithm proposed by Haam and
299 Huybers [2010] that tunes a record – stretches or contracts its time dimension
300 nonuniformly – to find the optimal match between the record and another time series.
301 The goodness of the match for a given tuning is measured by the covariance between the
302 tuned record and the other time series, and the optimal tuning is the one that maximizes
303 this covariance. In this case, the records are the synthetic PLDs, and they are tuned to
304 match the insolation function.

305 The DTW algorithm tunes the record to the forcing function by using a cost
306 matrix, which is constructed by computing the squared differences between each point in
307 the synthetic record and every point in the insolation function. The resulting matrix of
308 squared differences represents the costs (penalties) of all possible matches between points
309 in the two records. The algorithm then finds the path through the cost matrix that incurs
310 the lowest average cost, starting from an element that corresponds to the top of the PLD
311 record and the estimated time in the insolation function when the uppermost layer was
312 deposited, and ending at an element that corresponds to the bottom of the PLD record and
313 the time in the insolation function when the first layer was deposited. The calculated path
314 represents the tuned record that has the maximum possible covariance with the insolation
315 function. Figure 5 shows an example of an output of the DTW algorithm with both the
316 tuned and actual time-depth curves. The least-cost path is not required to terminate with
317 the earliest time in the insolation function; since most troughs only expose the uppermost

318 few hundred meters of stratigraphy out of a total of ~2km, it is likely that exposed
319 deposits only correspond to a fraction of the 5 Myr insolation function. Similarly, the
320 path is not required to start at the present day, because the uppermost strata may have
321 formed some time before the present. However, we expect that the age of the bottom of a
322 PLD sequence is much less certain than the age of the top, so we do not allow the starting
323 point of the least-cost path to vary as freely as the ending point. This is implemented by
324 imposing a non-zero cost on the leftmost column of the cost matrix and no cost on the
325 rightmost column (Fig. 5). We also impose a non-zero cost on the bottom row because a
326 path traveling along that row would correspond either to the unlikely scenario of a thick
327 layer of ice deposited instantaneously at the present day or to the unphysical scenario of
328 strata that are younger than the present.

329

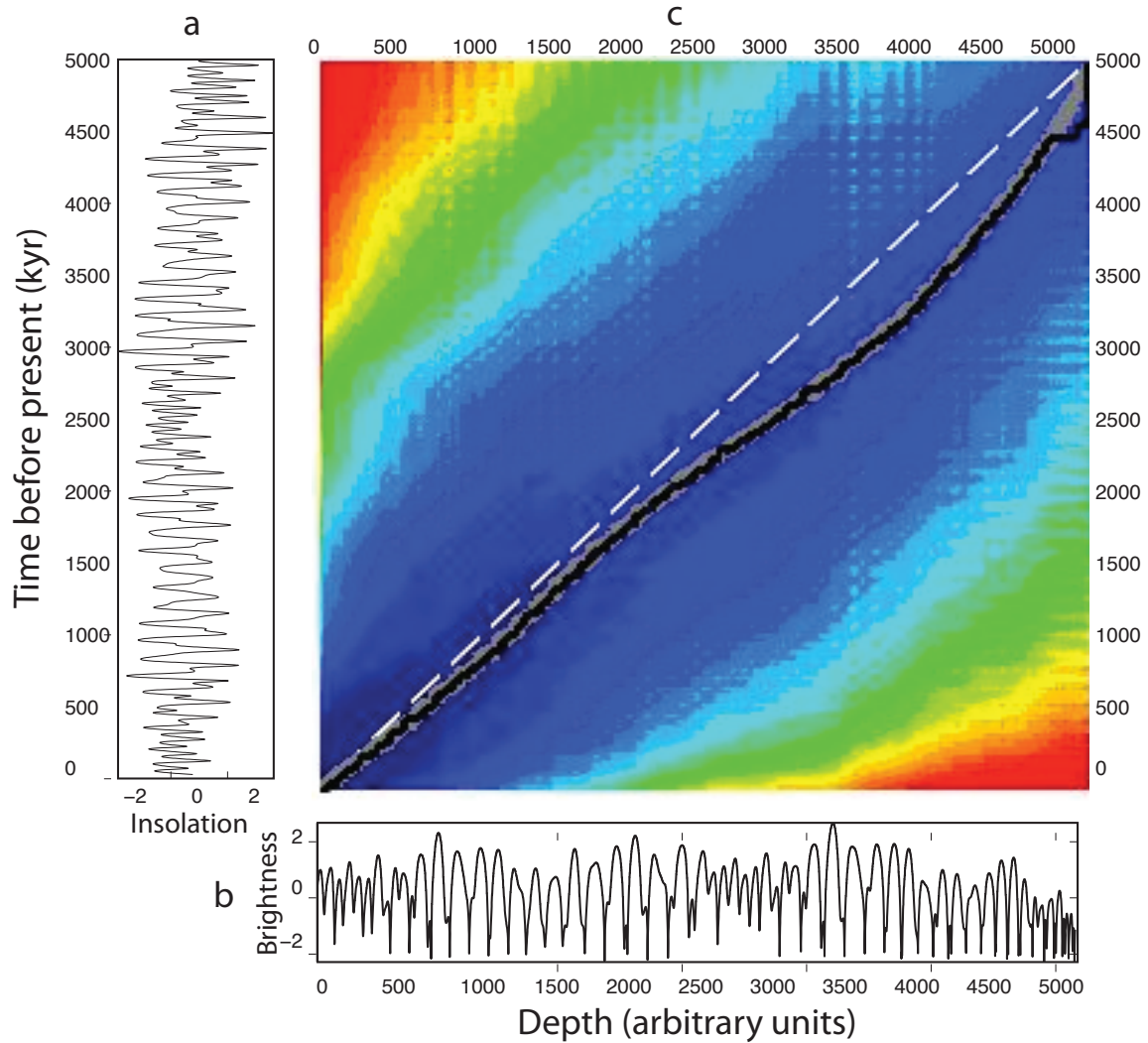


Figure 5. Output from the dynamic time warping algorithm comparing (a) the last five million years of Martian insolation history to (b) a synthetic PLD sequence. Both time series are normalized to unit variance. In the model, ice deposition stops (but without ablation) above a threshold insolation of 350 W/m^2 . The square region (c) corresponds to the cost matrix. The black line in (c) shows the path through the cost matrix that incurs the lowest average cost, and represents the tuned synthetic PLD. The colors represent cost, with warm colors indicating areas of higher cost and cool colors indicating areas of lower cost. The dashed line in (c) is simply the diagonal of the cost matrix, which represents a linear time-depth relationship. The gray line in (c) represents the true time-depth relationship for this synthetic PLD. The covariance for this tuning is 0.963 despite the hiatuses in deposition.

330

331 *3.2 Monte Carlo procedure*

332 The DTW algorithm gives the maximum covariance between a tuned synthetic
333 PLD and the insolation time series, but does not assign a statistical significance to that
334 covariance. The procedure therefore requires an additional step that quantitatively
335 evaluates the null hypothesis that the PLD record is a random time series uncorrelated
336 with insolation, and that the maximum covariance between the PLD and insolation is no
337 better than that obtained by chance. We evaluate this null hypothesis through a Monte
338 Carlo procedure in which random records with statistical characteristics similar to those
339 of the synthetic PLDs are tuned to match the insolation function. For each synthetic
340 PLD, 1000 random records with the same mean, variance, and lag-1 autocorrelation as
341 the synthetic PLD are generated. The DTW procedure then tunes each random record to
342 the insolation record using the same procedure applied to the synthetic PLD, yielding a
343 maximum covariance for each random record. A comparison of the resulting distribution
344 of 1000 maximum covariances with the maximum covariance between the insolation and
345 synthetic PLD provides a way of gauging the likelihood that the match is not spurious,
346 and therefore the confidence level at which the null hypothesis can be rejected. An
347 example is shown in Figure 6. We express this confidence level as the percentage of
348 random Monte Carlo records, P_{MC} , that yield a smaller maximum covariance than the
349 synthetic record. If $P_{MC} = 100\%$, then the synthetic PLD matches insolation better than
350 all random records, and the orbital signal is detected in the synthetic PLD with an
351 extremely high degree of confidence. If $P_{MC} = 50\%$, then the orbital signal is so obscured
352 by the PLD formation mechanism that the tuned match between the PLD and insolation is
353 no better than the median match between a random time series and insolation, and thus
354 there is little confidence that the modeled stratigraphy is related to insolation. Between

355 these two extremes is a range of confidence levels for detection of an orbital signal. This
 356 approach provides a way of quantifying the feasibility of detecting an orbital signal given
 357 a hypothesized PLD formation mechanism, as well as a way of quantifying the
 358 significance of orbital tuning applied to real PLD records, for which the formation
 359 mechanism is unknown. Figure 7 compares dynamic time warping analyses of synthetic
 360 PLD models and random time series for one case in which the covariance between
 361 insolation and the tuned PLD is substantially higher than for the tuned random time series
 362 (Fig. 7a,b) and another in which the PLD and random time series yield comparable
 363 covariances (Fig. 7c,d).

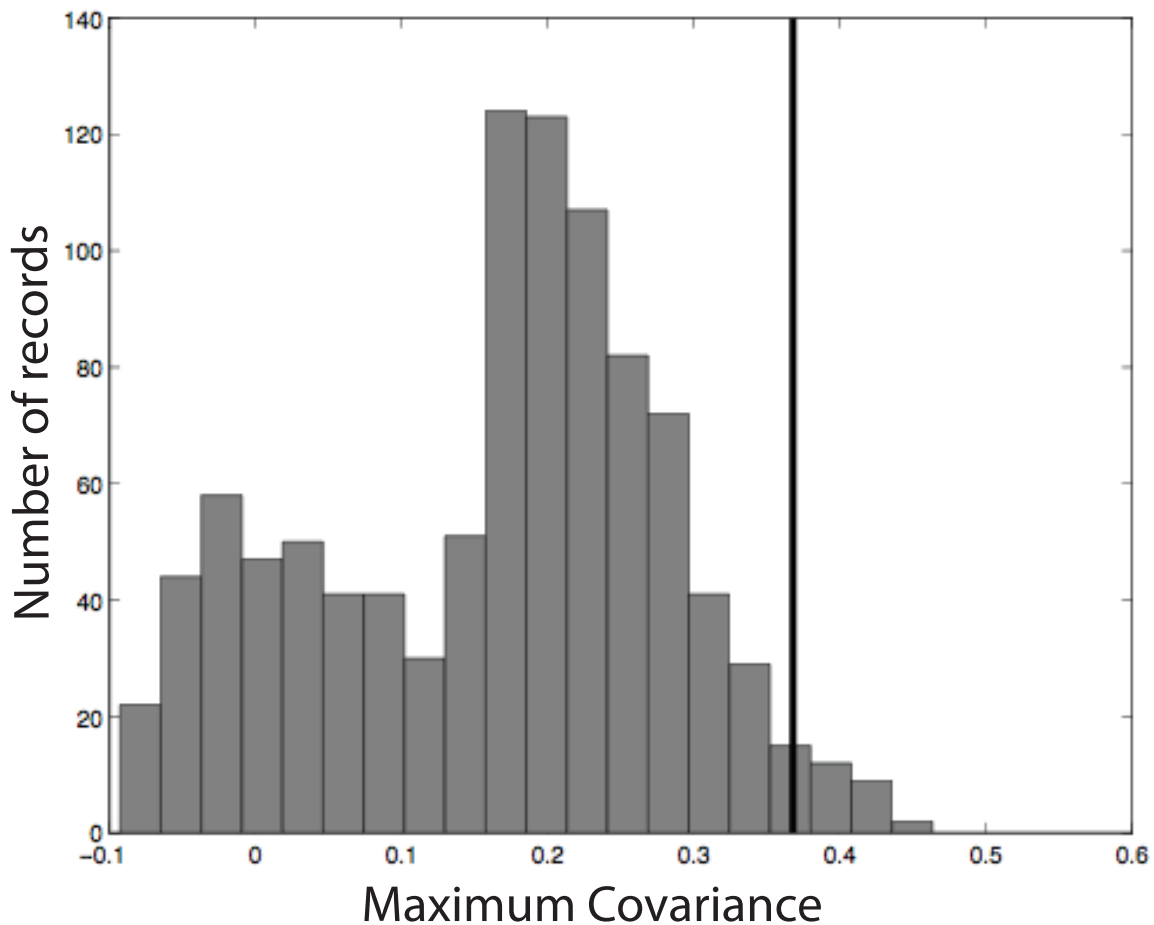


Figure 6. Histogram showing the distribution of maximum covariances for random records

generated from a synthetic PLD where ablation occurs at a threshold insolation value of 270 W/m². The maximum covariance for the synthetic PLD tuned to the insolation record is 0.368 (shown here as the vertical black line), which is greater than 97.2% of the maximum covariances of the random records. We consider this a confident detection of the orbital signal.

364

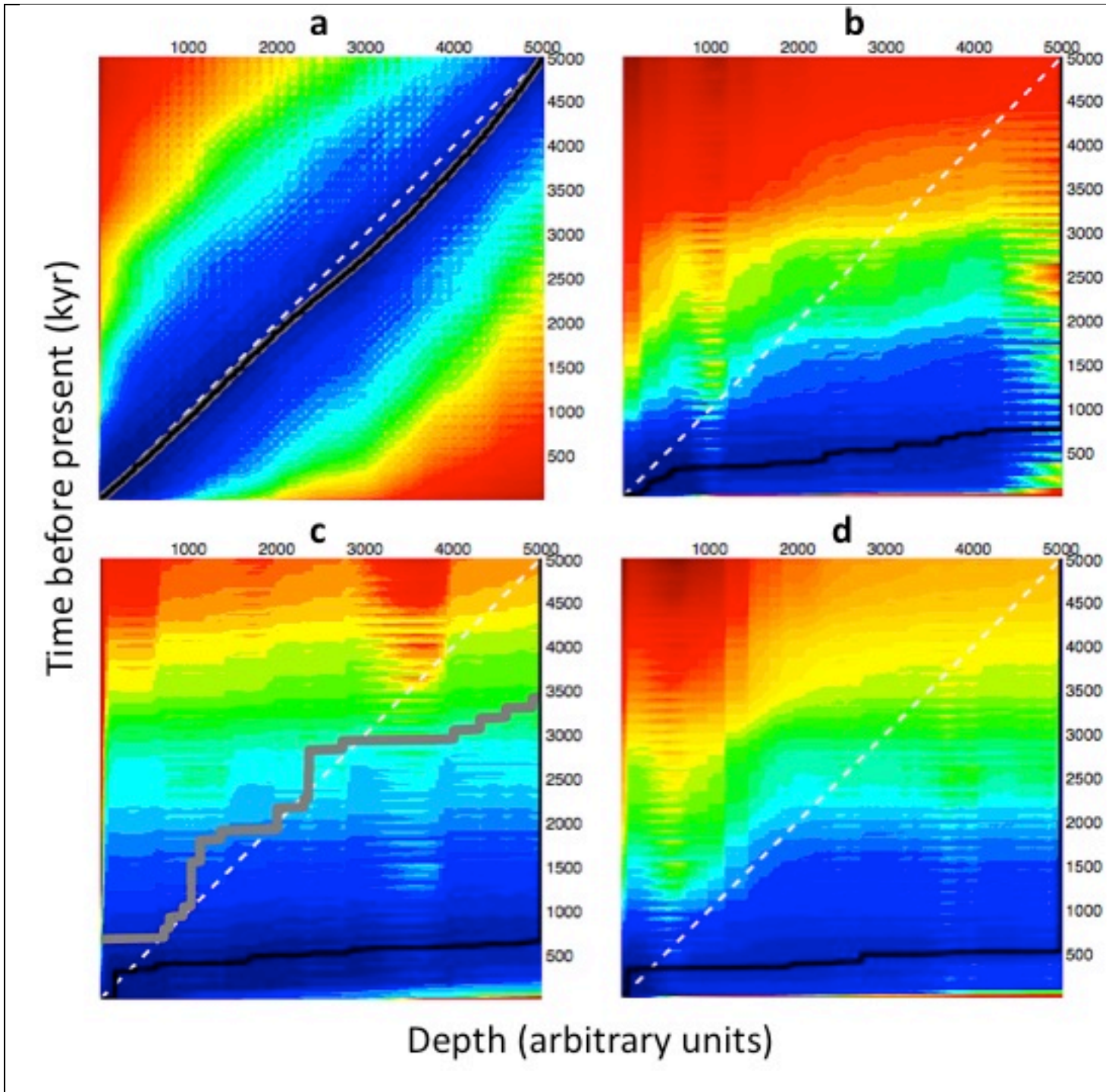


Figure 7. Cost matrices, as shown in Fig. 5, for four different dynamic time warping analyses. Plot (a) shows a synthetic PLD formed over 5 Myr where ablation occurs at a threshold insolation value of 350 W/m^2 tuned to a 5 Myr insolation signal. Plot (b) shows a corresponding random PLD tuned to the same signal. Plot (c) shows a synthetic PLD formed over 5 Myr where ablation occurs at a threshold insolation value of 250 W/m^2 tuned to a 5 Myr insolation signal. Plot (d) shows a corresponding random PLD tuned to the same signal. Note that the tuning in plot (a) is significantly better than that in plot (b), but there is no significant difference between plots (c) and (d). Solid black lines are the tuned time-depth relationships, gray lines are the true time-depth relationships of the synthetic PLDs, and colors represent higher (warm colors) and lower (cool colors) costs, as in Fig. 5.

365

366

367 4. Results*368 4.1 Qualitative characteristics of synthetic PLD stratigraphy*

369 Model outputs of synthetic PLD records yield noteworthy trends, even before
370 application of the DTW algorithm and Monte Carlo procedure. In the no-hiatus case,
371 where ice deposition rate varies linearly with insolation and is always positive (Fig. 4a,b),
372 varying the coefficient relating ice deposition rate to insolation changes the absolute
373 values of dust concentration in the resultant stratigraphic sequences, but not the relative
374 frequencies of bedding. The outcome of this simple formation model is therefore
375 qualitatively independent of model parameters.

376 The relative frequencies of bedding in models that allow hiatuses are also
377 insensitive to changes in the coefficient relating ice deposition rate to insolation (Fig. 4c-
378 f). However, adjusting the threshold insolation value in these models does change the
379 stratigraphy qualitatively, because it influences the fraction of time that is preserved.
380 Figure 4g,h shows two instances of the model with hiatuses but no ablation, with
381 different thresholds for ice deposition. Note that adjustment of this threshold changes not
382 only the values of dust concentration, but the number of bright peaks as well.

383

384 4.2 Detection of orbital signals for different accumulation models

385 As mentioned in section 3, a maximum covariance was calculated for each
386 synthetic PLD and was then compared to the maximum covariances obtained for 1000
387 randomly generated records that shared several statistical properties with the synthetic

388 PLD. For models with no ablation and no hiatuses (Fig. 4a,b), the maximum covariance
389 is close to 1 and is always greater than the maximum covariances for all randomly
390 generated records ($P_{MC} = 100\%$). Thus, for this simple formation function, we can
391 confidently identify an orbital signal in all cases, despite a nonlinear time-depth
392 relationship that would complicate or preclude detection with conventional time series
393 analysis methods. This result illustrates one of the main benefits of the tuning procedure,
394 and suggests that tuning analyses of the PLDs, combined with an appropriate statistical
395 test, could reveal underlying structure that conventional time series analyses have missed.

396 For the more complicated models that produce hiatuses (Fig. 4c-f), P_{MC} generally
397 scales with the insolation threshold for ice deposition (Fig. 8a), because higher thresholds
398 result in shorter hiatuses. That is, when less of the insolation time series produces strata
399 that are preserved, the match between the PLDs and insolation is worse, and is less likely
400 to be better than the match to a random record. For sufficiently high insolation thresholds
401 ($> 225 \text{ W/m}^2$ for the model with hiatuses but no ablation, and $> 270 \text{ W/m}^2$ for the model
402 with ablation), the maximum covariance for the model output is greater than all
403 maximum covariances for random records ($P_{MC} = 100\%$), despite incomplete
404 preservation of the modeled time interval (Fig. 8a). Below those threshold insolation
405 values, P_{MC} decreases as the threshold is lowered. For models without ablation but with
406 ice deposition stopping above a threshold insolation value of 222 W/m^2 , an orbital signal
407 can be detected with a 95% degree of confidence. For a threshold insolation value of 174
408 W/m^2 or lower, P_{MC} is not significantly higher than 50%, and thus the model output can
409 not be tuned to an orbital signal better than a random record; detection of an orbital signal
410 is infeasible. For models with ablation above a threshold insolation value of 269 W/m^2 ,

411 an orbital signal can be detected with a 95% degree of confidence. For a threshold
412 insolation value of 243 W/m^2 or lower, P_{MC} is not significantly higher than 50%, and thus
413 the model output cannot be tuned to an orbital signal better than a random record;
414 detection of the signal is infeasible. For a threshold value of 210 W/m^2 or lower, no PLD
415 record exists – it is all ablated away.

416 We find that this relationship can be generalized by plotting P_{MC} as a function of
417 the fraction of time preserved in the stratigraphy (Fig. 8b). For the formation models
418 investigated here, the modeled PLDs can be distinguished from random time series (P_{MC}
419 $> 50\%$) even if only a few percent of the modeled time interval is preserved in the
420 stratigraphy, and can be confidently distinguished ($P_{MC} > 90\%$) if approximately 8-10%
421 of the time interval is preserved. Between these extremes, P_{MC} increases approximately
422 linearly with the fraction of time preserved.

423 We also examined the influence of the total duration of PLD accumulation on the
424 ease of identifying an orbital signal. In addition to the insolation time series for the past 5
425 Myr (Fig. 2), we drove the model that allows ablation with the insolation for the past 3
426 Myr and the past 1 Myr, and performed the same statistical analysis on the model
427 outputs. The results in Fig. 7 demonstrate that, in addition to the dependence on
428 insolation threshold, P_{MC} is higher when the total accumulation interval is longer:
429 depositing the PLDs over a longer period of time makes it easier to detect an orbital
430 influence.

431

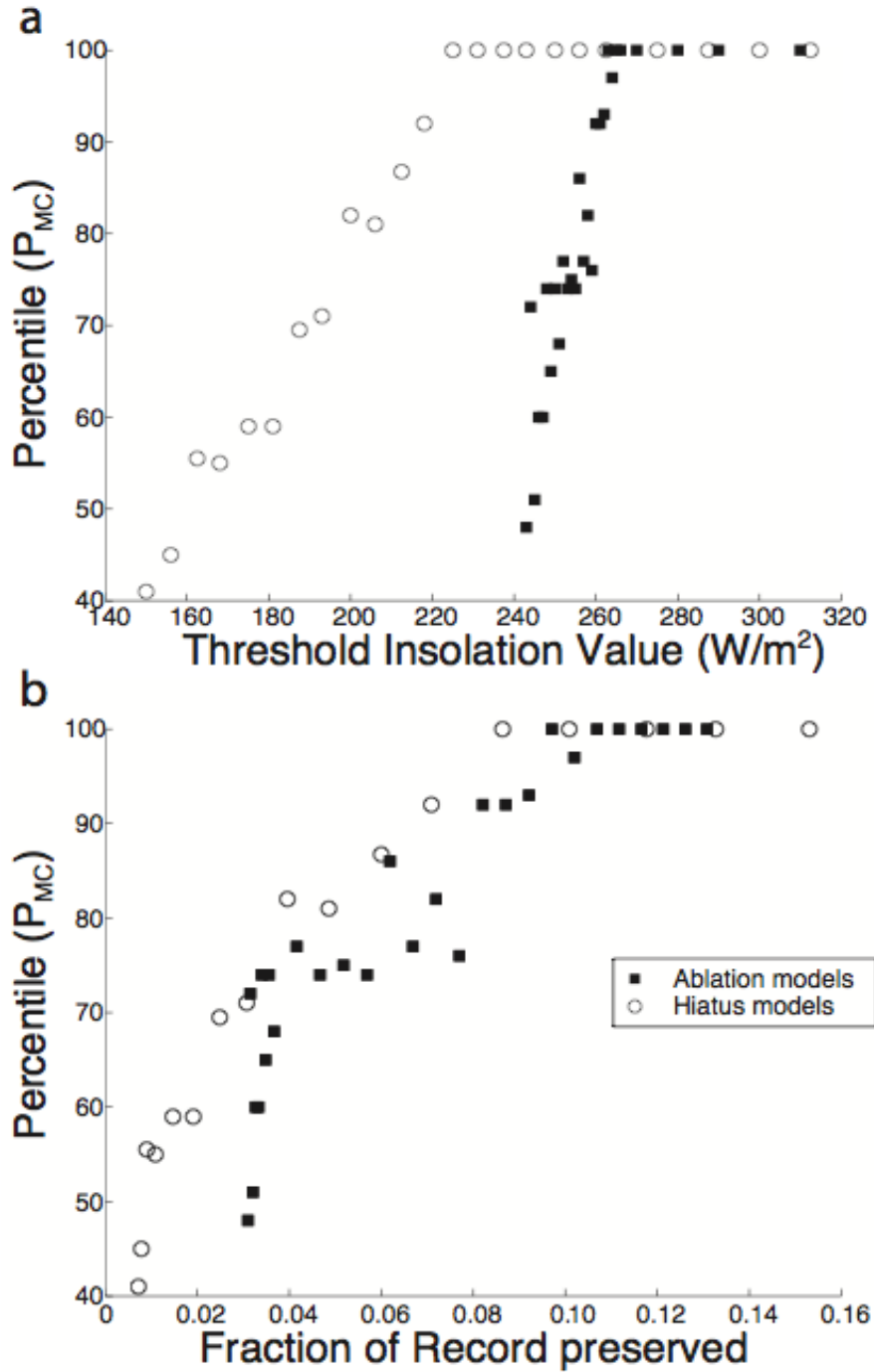


Figure 8. Percentage of randomly generated time series, P_{MC} , with insolation covariance that is smaller than the insolation covariance of a modeled PLD sequence, as a function of (a) the threshold insolation, and (b) the fraction of the 5 Myr time interval that is preserved in the modeled stratigraphy. Trends for the model with hiatuses but no ablation and the model with hiatuses that do include ablation differ when P_{MC} is compared with the magnitude of the insolation threshold for ice accumulation (a), but overlap when P_{MC} is compared with the fraction of time preserved (b).

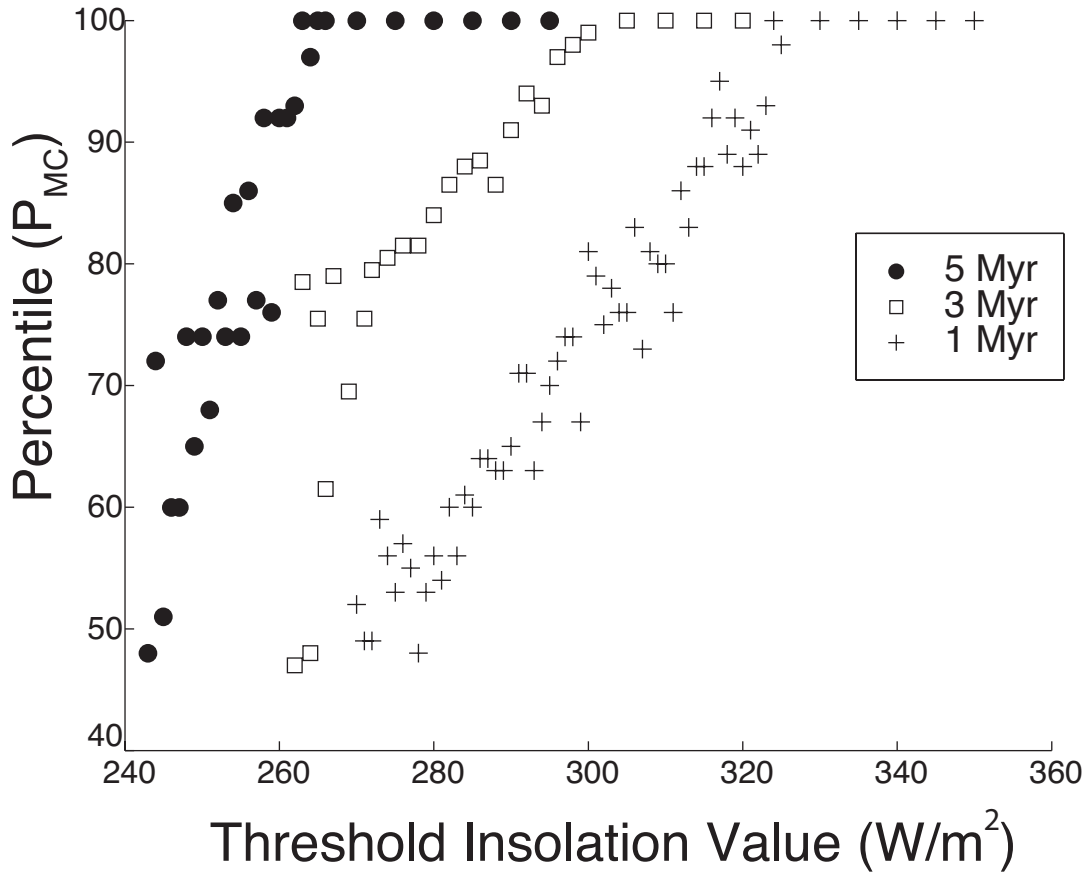


Figure 9. Percentage of randomly generated time series, P_{MC} , with insolation covariance that is smaller than the insolation covariance of a modeled PLD sequence, as a function of the insolation threshold for ice accumulation in the model that allows ablation. Different symbols correspond to models in which PLDs are deposited over the past 5, 3, or 1 million years of Martian history.

433

434

435 **5. Discussion**

436 *5.1 Feasibility of identifying an orbital signal through tuning*

437 In general, our results imply that detection of an orbital influence on PLD
 438 formation is feasible (though not trivial), even if the relationship between depth and time
 439 in the stratigraphy is strongly nonlinear. Indeed, we find that PLD sequences formed by
 440 ice and dust deposition models that include no hiatuses in deposition can be distinguished
 441 from stochastic time series 100% of the time. While such a deposition model is probably

442 overly simple (see section 5.3), this result nonetheless emphasizes that a nonlinear time-
443 depth relationship is not an insurmountable complication.

444 In the more likely scenario that the PLD stratigraphy contains gaps, our analysis
445 provides a framework for determining whether the accumulated record contains enough
446 information to reliably identify orbital influence. Features such as unconformities and
447 crosscutting troughs suggest that the accumulation of the polar stratigraphic record was
448 punctuated by periods of no ice deposition [Tanaka et al., 2008]. In models with hiatuses
449 or ablation, the ability to detect orbital signals is a function of the threshold insolation at
450 which ice deposition stops. This result makes intuitive sense: when more of a PLD
451 record is ablated away, it is more difficult to detect the underlying forcing that drove PLD
452 formation. Our procedure identifies a clear, roughly linear relationship between the ease
453 of identifying an orbital influence, as measured by P_{MC} , and the insolation threshold for
454 ice deposition in each model (Fig. 8a). However, these particular values of the insolation
455 threshold should not be interpreted as absolute, because the true relationships between
456 insolation and ice and dust deposition rates are unknown. Instead, we emphasize that the
457 fraction of time preserved in the stratigraphy is the more relevant quantity for
458 determining whether an orbital signal can be confidently detected. The clearest
459 demonstration of this point is that the trends in P_{MC} for the different models collapse to a
460 more uniform trend when plotted against fraction of time preserved (Fig. 8b) rather than
461 the threshold insolation (Fig. 8a).

462 The other main factor that influences the ease of detecting orbital influence is the
463 total duration of PLD formation. In general, the shorter the time period over which the
464 PLDs form, the more difficult it is to detect an orbital signal in the stratigraphy (Fig. 9).

465 This too makes intuitive sense: a stratigraphic sequence that preserves 50% of five
466 million years contains more information than a sequence that preserves 50% of one
467 million years, and the additional information makes it easier to distinguish the orbitally
468 driven record from a random record.

469

470 *5.2 Fraction of time preserved in the polar cap stratigraphy*

471 Although the northern polar cap of Mars is thought to have experienced net
472 accumulation of ice over the past few Myr [Pollack, et al., 1979; Kieffer, 1990; Laskar et
473 al., 2002], it is unclear whether the cap is presently in a state of net accumulation or net
474 ablation. If we assume that Mars is in a state of net ablation today, then our models
475 suggest that the current PLDs represent only a small fraction ($< 10\%$) of the total record
476 deposited over time. The current insolation at the Martian north pole during the summer
477 solstice, 265 W/m^2 , is near the mean insolation for the past 5 Myr of Martian history (Fig.
478 2). Thus, if the PLDs are ablating today, it is likely that they have ablated more often than
479 they have accumulated, and their strata may only record a small fraction of the past 5
480 Myr. It should be noted, however, that these models assume ablation occurs at a similar
481 rate to ice deposition. If ablation is much slower than ice deposition (which might be the
482 case if, for example, ablation forms a dust lag that inhibits further ablation), the PLDs
483 could record a larger portion of recent Martian history, even if the caps are experiencing
484 net ablation today.

485

486

487

488 *5.3 Additional considerations for modeling PLD formation*

489 The objective of this study is to identify the main factors that influence the
490 viability of orbital tuning applied to the PLDs. We therefore have not attempted to
491 formulate a model for PLD accumulation that incorporates all the factors that influence
492 the appearance of the stratigraphy, nor have we attempted an absolute calibration of rate
493 parameters. Nonetheless, given the finding that orbital tuning may indeed be a viable
494 means of identifying the cause of paleoclimate signals preserved in the PLDs, it is
495 important to consider the limitations of, and possible improvements to, the simple models
496 presented here.

497 Several improvements could be implemented to make the PLD formation models
498 more realistic. In particular, both ice and dust deposition rates could be expressed in
499 terms of a fuller complement of physical variables. Ice deposition rates could take
500 humidity into account. Dust deposition rates could consider the occurrence of global dust
501 storms, which historical observations [Pollack et al., 1979; Toon et al., 1980; Haberle,
502 1896; Zurek and Martin, 1993] suggest produce a high frequency signal, but which may
503 also include long-term trends related to insolation [Fernandez, 1998]. These additional
504 complexities will almost certainly make detection of an orbital signal more difficult, and
505 thus the confidence in detection abilities presented in this study should be interpreted as
506 an upper limit.

507 Other potential complications are the possibility of stochastic variability in
508 deposition processes and the imperfect relationship between PLD composition and
509 appearance. To explore how these factors influence the orbital tuning procedure, we
510 performed an additional analysis in which the modeled ice deposition rate includes a

511 stochastic component. Specifically, we added red noise (a random signal in which
512 spectral power P declines with frequency f according to $P \propto f^{-2}$) to the amount of ice
513 deposited in a given time step in our models to generate synthetic PLDs that are not
514 constructed with the assumption of a deterministic relationship between ice deposition
515 rate and insolation. Starting with a model that forms hiatuses when the insolation is 300
516 W/m^2 or greater, we varied the amplitude of the noise and produced 100 random
517 realizations of the PLD strata for each value of noise amplitude. We then used the DTW
518 algorithm to calculate the maximum covariance between each modeled stratigraphic
519 sequence and the insolation time series. Figure 10 shows how the maximum covariance
520 depends on the amplitude of the noise. The addition of red noise to the ice deposition
521 rate changes the maximum covariance in a gradual fashion, suggesting that a non-
522 deterministic relationship between insolation and PLD accumulation does not necessarily
523 prevent the DTW method from identifying an orbital signal.

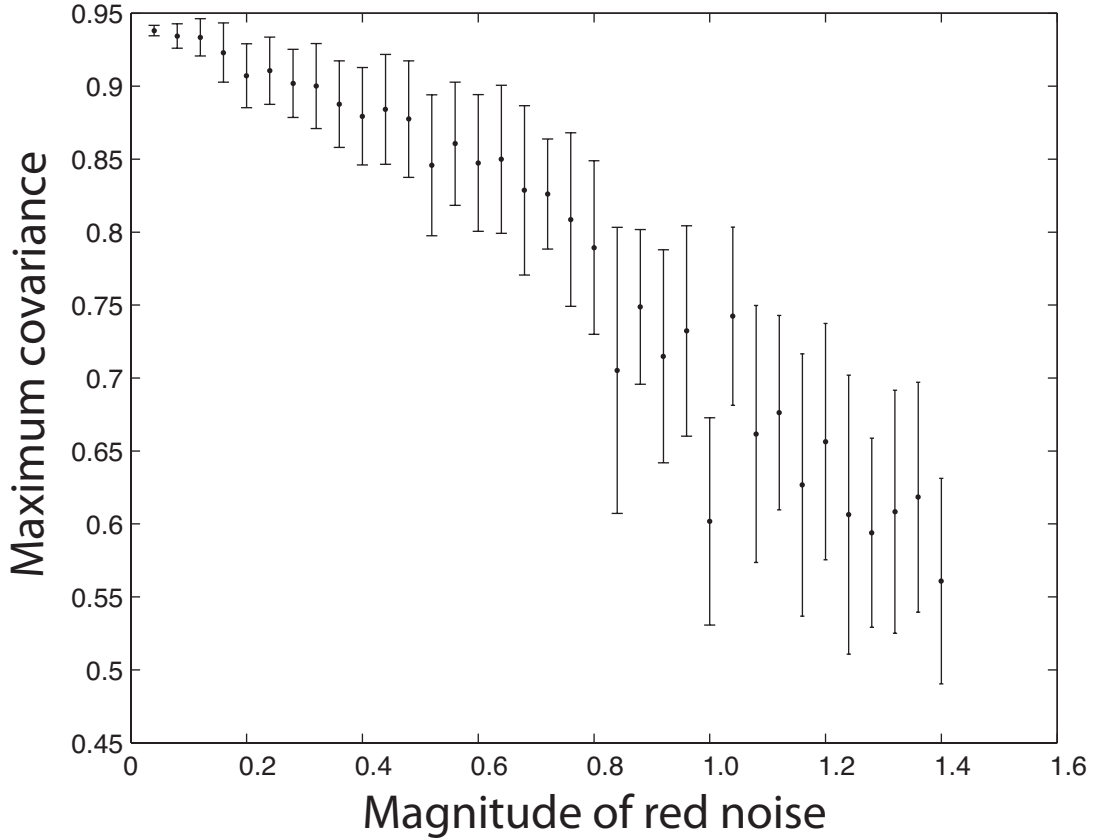


Figure 10. Effect of adding red noise to the modeled ice deposition rate on the dynamic time warping algorithm’s ability to tune the resulting synthetic PLD to the insolation signal. The magnitude of the noise added is the ratio of the variance of the noise to the variance of the ice deposition rate. Each point represents the average maximum covariance of 100 different tunings of a synthetic PLD that contains hiatuses when the insolation reaches a value of 300 W/m^2 or greater. Error bars are one standard deviation.

524

525

526 *5.4 Implications for orbital tuning of the observed PLD stratigraphy*

527 Given the probable influence of insolation on the deposition or ablation of water

528 ice, the major constituent of the PLDs, it is likely that the relationship between time and

529 depth in the PLDs is nonlinear, as our simple models predict. One of the main

530 implications of our results is that it may nonetheless be possible to identify evidence of

531 quasi-periodic insolation forcing by applying a tuning procedure like the one described

532 here. Such an analysis could reveal coherent signals in the PLD stratigraphy that would
533 not be detected by conventional time series analysis procedures that assume a linear or
534 nearly linear time-depth relationship [Perron and Huybers, 2009].

535 The appropriate future direction of this study is to apply the statistical analysis
536 described here to actual images of the Martian PLDs. Images obtained by the Mars
537 Orbiter Camera (MOC) on the Mars Global Surveyor spacecraft and the High Resolution
538 Imaging Science Experiment (HiRISE) aboard the Mars Reconnaissance Orbiter can be
539 converted to sequences of brightness vs. depth that can be analyzed with the same
540 procedure as the synthetic sequences of dust concentration studied here [Milkovich and
541 Head, 2005; Milkovich et al., 2008; Perron and Huybers, 2009; Fishbaugh, 2010; Limaye
542 et al., 2012]. These sequences can be compared to insolation records of varying lengths,
543 with the important consideration that a match would only determine the age of the
544 exposed sequence; such an age would be younger than that of the entire PLDs, which
545 would need to be extrapolated. It should be noted that conversion of images to
546 brightness-depth sequences introduces an additional source of noise that must be
547 considered [Tanaka, 2005], but recent efforts to quantify these uncertainties have found
548 them to be modest [Limaye et al., 2012]. The dynamic time warping procedure we have
549 applied to brightness records can in principle be applied to other proxies for PLD
550 composition, such as sequences of slope or roughness vs. depth, or composite records
551 incorporating both brightness and topographic information. Thus, for any possible
552 identification of an orbital signal in the PLDs, the statistical procedure presented here can
553 yield a quantitative estimate of the likelihood of a spurious match. If the PLDs preserve a
554 sizeable fraction of the total accumulation time, and the deposition rates of ice and dust

555 are sufficiently deterministic, it may well be possible to detect an orbital signal, if one is
556 present.

557

558 **6. Conclusions**

559 We use a statistical procedure that evaluates the significance of time series tuning
560 to examine the feasibility of detecting an influence of orbital variations on the polar
561 stratigraphy of Mars. We apply the procedure to synthetic stratigraphic sequences
562 generated by simple formation models for the Martian polar layered deposits, and find
563 that detection of an orbital signal in the resulting stratigraphy is feasible, though not
564 trivial. Models in which ice deposition rate varies linearly with insolation produce
565 stratigraphy in which orbital signals are easily detected with the tuning procedure, despite
566 a nonlinear relationship between depth and time that can foil conventional time series
567 analysis methods. For more complicated models of ice deposition, detection ability
568 depends strongly on the threshold insolation at which ice deposition stops or an ablation
569 episode begins, and more generally, on the fraction of total formation time preserved in
570 the strata. Improved constraints on ice and dust deposition rates on Mars would permit a
571 more definitive assessment of whether detection of an orbital signal in the PLDs is
572 feasible, but our analysis does not reveal the problem to be necessarily intractable at the
573 current state of knowledge. HiRISE images should be adequate to identify evidence of
574 an orbital influence if PLD formation is controlled by a sufficiently simple mechanism,
575 but for certain formation scenarios described here, confident identification of an orbital
576 signal is impossible without absolute ages, no matter the quality of the spacecraft images.
577

578 **Acknowledgments**

579 This study was supported by the NASA Mars Data Analysis Program, award 65P-
580 1089493.

581

582 **References**

- 583 Banks, M.E., et al., 2010. *Crater population and resurfacing of the Martian north polar*
584 *layered deposits*. *J. Geophys. Res.* 115, E08006, doi:10.1029/2009JE003523.
- 585 Berger, A.L., 1978. *Long-term variations of daily insolation and Quaternary climatic*
586 *changes*. *J. Atmos. Sci.* 35, 2362-2367
- 587 Byrne, S., 2009. *The Polar Deposits of Mars*. *Annu. Rev. Earth Planet. Sci* 37, 535-560.
- 588 Cutts, J.A., 1973. *Nature and origin of layered deposits of the Martian polar region*. *J.*
589 *Geophys. Res.* 78, 4231-4249.
- 590 Cutts, J.A. et al., 1976. *North Polar Region of Mars: Imaging results from Viking 2*.
591 *Science* 194, 1329-1337.
- 592 Cutts, J.A., and Lewis, B.H., 1982. *Models of Climate Cycles Recorded in Martian Polar*
593 *Layered Deposits*. *Icarus* 50, 216-244.
- 594 Fernandez, W, 1998. *Martian Dust Storms: A Review*. *Earth, Moon, and Planets* 77,
595 19-46.
- 596 Fishbaugh, K.E., and Hvidberg, C.S., 2006. *Martian north polar layered deposits*
597 *stratigraphy: Implications for accumulation rates and flow*. *J. Geophys. Res.* 111.
- 598 Fishbaugh, K.E., et al., 2010. *First high-resolution stratigraphic column of the Martian*
599 *north polar layered deposits*. *Geophys. Res. Letters* 37.
- 600 Forget, F. et al., 2006. *Formation of glaciers on Mars by atmospheric precipitation at*
601 *high obliquity*. *Science* 311, 368-371.
- 602 Haam, E., and Huybers, P., 2010. *A test for the presence of covariance between time-*
603 *uncertain series of data with application to the Dongge Cave speleothem and*
604 *atmospheric radiocarbon records*. *Paleoceanography* 25.
- 605 Haberle, R.M., 1986. *Interannual variability of global dust storms on Mars*. *Science*
606 234, 459-461.
- 607 Hays, J.D., Imbrie, J., and Shackleton, N.J., 1976. *Variations in the Earth's orbit:*
608 *Pacemaker of the Ice Ages*. *Science* 194, 1121-1132.
- 609 Herkenhoff, K., and Plaut, J.J., 2000. *Surface ages and resurfacing rates of the polar*
610 *layered deposits on Mars*. *Icarus* 144, 243-253.
- 611 Herkenhoof, K.E., et al., 2007. *Meter-scale morphology of the north polar region of*
612 *Mars*. *Science* 317, 1711-1715.
- 613 Howard, A.D., Cutts, J.A., and Blasius, K.R., 1982. *Stratigraphic relationships between*
614 *Martian polar cap deposits*. *Icarus* 50, 161-215.
- 615 Jakosky, B.M., Henderson, B.G., and Mellon, M.T., 1995. *Chaotic obliquity and the*
616 *nature of the Martian Climate*. *J. Geophys. Res.* 100, 1579-1594.
- 617 Kieffer, H.H, 1990. *H₂O grain size and the amount of dust in Mars residual north polar*
618 *cap*. *J. Geophys. Res.* 95, 1481-1493.

- 619 Kominz, M.A., and Piasias, N.G., 1979. *Pleistocene climate: Deterministic or*
620 *stochastic?* *Science* 204, 171-173.
- 621 Koutnik, M., Byrne, S., and Murray, B., 2002. *South Polar Layered Deposits of Mars:*
622 *The cratering record.* *J. Geophys. Res.*, 107, 5100, doi:10.1029/2001JE001805.
- 623 Laskar, J. et al., 2004. *Long term evolution and chaotic diffusion of the insolation*
624 *quantities of Mars.* *Icarus* 170: 343-64.
- 625 Laskar, J., Levrard, B., and Mustard, J.F., 2002. *Orbital forcing of the Martian polar*
626 *layered deposits.* *Nature* 419, 375-377.
- 627 Laskar, J., and Robutel, P., 1993. *The chaotic obliquity of the planets.* *Nature* 361,
628 608-612.
- 629 Levrard, B., et al., 2007. *Recent formation and evolution of northern Martian polar*
630 *layered deposits as inferred from a Global Climate Model.* *J. Geophys. Res.* 112.
- 631 Limaye, A.B.S., O. Aharonson and J.T. Perron. *Detailed stratigraphy and bed thickness*
632 *of the Mars north and south polar layered deposits.* *J. Geophys. Res.*, in review,
633 2012.
- 634 Lisiecki, L. E., and P. A. Lisiecki, 2002, *Application of dynamic programming to the*
635 *correlation of paleoclimate records.* *Paleoceanography*, 17(D4), 1049.
- 636 Mellon, M.T., 1996. *Limits on the CO₂ content of the Martian polar layered deposits.*
637 *Icarus* 124, 268-279.
- 638 Milkovich S.M., and Head J.W. III, 2005. *North polar cap of Mars: Polar layered*
639 *deposit characterization and identification of a fundamental climate signal.* *J.*
640 *Geophys. Res.* 110, 1005
- 641 Milkovich, S.M., et al., 2008. *Stratigraphic analysis of the northern polar layered*
642 *deposits of Mars: implications for recent climate history.* *Planetary and Space*
643 *Science* 56(2), 266-288.
- 644 Mischna, M.A., et al., 2003. *On the orbital forcing of Martian water and CO₂ cycles: A*
645 *general circulation model study with simplified volatile schemes.* *J. Geophys.*
646 *Res.* 108, 5062.
- 647 Murray, B.C. et al., 1972. *Geological Framework of the South Polar Region of Mars.*
648 *Icarus* 17, 328-345.
- 649 Murray, B.C., Ward, W.R., and Yeung S.C., 1973. *Periodic insolation variations on*
650 *Mars,* *Science* 180, 638-640.
- 651 Nye, J.F. et al., 2000. *The instability of a south polar cap on Mars composed of carbon*
652 *dioxide.* *Icarus* 144, 449-455.
- 653 Perron, J.T., and Huybers, P, 2009. *Is there an orbital signal in the polar layered*
654 *deposits on Mars?* *Geology* 37, 155-158.
- 655 Phillips, R.J. et al., 2008. *Mars north polar deposits: Stratigraphy, age, and*
656 *geodynamical response.* *Science* 320, 1182-1185.
- 657 Pollack, J.B. et al., 1979. *Properties and effects of dust particles suspended in the*
658 *Martian atmosphere.* *J. Geophys. Res.* 84, 2929-2945.
- 659 Plaut, J.J. et al., 2007. *Subsurface radar sounding of the south polar layered deposits of*
660 *Mars.* *Science* 316, 92-96.
- 661 Picardi, G. et al., 2005. *Radar soundings of the subsurface of Mars.* *Science* 310,
662 1925-1928.
- 663 Proistosescu, C., P. Huybers and A.C. Maloof, 2012. *To Tune or not to Tune: Detecting*
664 *Orbital Variability in Oligo-Miocene Climate Records.* *Earth and Planetary*

- 665 Science Letters, 325–326, 100–107.
666 Sadler, P.M., 1981. *Sediment accumulation rates and the completeness of stratigraphic*
667 *sections*, J. Geol. 89, 569-584.
668 Smith, D.E., Zuber, M.T., and Neumann, G.A., 2001. *Seasonal variations of snow depth*
669 *of Mars*. Science 294, 2141-2145.
670 Tanaka, K.L., 2005. *Geology and insolation-driven climatic history of Amazonian north*
671 *polar materials on Mars*. Nature 437, 991-994.
672 Tanaka, K.L. et al., 2008. *North polar region of Mars: Advances in stratigraphy,*
673 *structure, and erosional modification*. Icarus 196, 318-358.
674 Thomas, P. et al., 1992. *Polar deposits of Mars* in Kieffer, H.H., et al., *Mars*. Tucson,
675 University of Arizona press, 767-795.
676 Toon, O.B. et al., 1980. *The astronomical theory of climatic change on Mars*. Icarus 44,
677 552-607.
678 Touma, J., and Wisdom, J., 1993. *The chaotic obliquity of Mars*. Science 259,
679 1294-1297.
680 Ward, W.R., 1973. *Large-scale variations in the obliquity of Mars*, Science 181,
681 260-262.
682 Ward, W. R., 1974, *Climatic variations on Mars: 1. Astronomical theory of insolation*.
683 J. Geophys. Res., 79, 3375 – 3386.
684 Ward, W. R., 1992, *Long-term orbital and spin dynamics of Mars*, in *Mars*, edited by H.
685 H. Kieffer et al., chap. 9, pp. 298 – 320, Univ. of Ariz. Press, Tucson.
686 Weedon, G., 2003. *Time-Series Analysis and Cyclostratigraphy*. Cambridge, Cambridge
687 University Press.
688 Wieczorek, M.A., 2008. *Constraints on the composition of the martian south polar cap*
689 *from gravity and topography*. Icarus 196, 506-517.
690 Wunsch, C., 2004. *Quantitative estimate of the Milankovitch-forced contribution to*
691 *observed Quaternary climate change*, Quaternary Sci. Rev. 23, 1001-1012.
692 Zurek, R., and Martin, L., 1993. *Interannual variability of planet-encircling dust storms*
693 *on Mars*. J. Geophys. Res. 98, 3247-3259.
694 Zuber, M.T. et al., 1998. *Observations of the north polar region of Mars from the Mars*
695 *orbiter laser altimeter*. Science 282, 2053-2060.
696 Zuber, M.T., et al., 2007. *Density of Mars' south polar layered deposits*. Science 300,
697 299-303.
698
699
700